J. Fluid Mech. (1992), *vol.* 236, *pp.* 535–556
Printed in Great Britain

Spiralling columnar convection in rapidly rotating spherical fluid shells

By K. ZHANG†
Department of Earth Sciences, University of Leeds, Leeds LS2 9JT, UK

(Received 10 July 1990 and in revised form 2 August 1991)

It is shown that the fundamental features of both thermal instabilities and the corresponding nonlinear convection in rapidly rotating spherical systems (in the range of the Taylor number $10^9 < T < 10^{12}$) are determined by the fluid properties characterized by the size of the Prandtl number. Coefficients of the asymptotic power law for the onset of convection at large Taylor number are estimated in the range of the Prandtl number $0.1 \leqslant Pr \leqslant 100$. For fluids of moderately small Prandtl number, a new type of convective instability in the form of prograde spiralling drifting columnar rolls is discovered. The linear columnar rolls extend spirally from near latitude 60° to the equatorial region, and each spans azimuthally approximately five wavelengths with the inclination angle between a spirally elongated roll and the radial direction exceeding 45°. As a consequence, the radial lengthscale of the linear roll becomes comparable with the azimuthal lengthscale. A particularly significant finding is the connection between the new instability and the predominantly axisymmetric convection. Though non-axisymmetric motions are preferred at the onset of convection, the nonlinear convection (at the Rayleigh number of the order of $(R-R_c)/R_c = O(0.1)$) bifurcating supercritically from the spiralling mode is primarily dominated by the component of the axisymmetric zonal flow, which contains nearly 90% of the total kinetic energy. For fluids of moderately large Prandtl numbers, thermal instabilities at the onset of convection are concentrated in a cylindrical annulus coaxial with the axis of rotation; the position of the convection cylinder is strongly dependent on the size of the Prandtl number. The associated nonlinear convection consists of predominantly non-axisymmetric columnar rolls together with a superimposed weak mean flow that contains less than 10% of the total kinetic energy at $(R-R_c)/R_c = O(0.1)$. A double-layer structure of the temperature field (with respect to the basic state) forms as a result of strong nonlinear interactions between the nonlinear flow and the temperature field. It is also demonstrated that the aspect ratio of the spherical shell does not substantially influence the fundamental properties of convection.

1. Introduction

In rotating spherical fluid systems, axisymmetric zonal flows showing differential rotation, i.e. deviating from a state of a rigid-body rotation, are encountered in many geophysical and astrophysical phenomena. Much of the interest in the previous work (e.g. Busse 1970*b*; Gilman 1977; Hart, Glatzmaier and Toomre 1986) on nonlinear spherical convection stems from the desire to provide an explanation for differential

† Present address: Department of Mathematics, University of Exeter, Exeter, EX4 4QJ, UK.

rotation, such as the solar differential rotation with faster flows in the equatorial region. Differential rotation within the fluid core of the earth and the solar convection zone certainly play a major role in generating the toroidal component of their respective magnetic fields (Moffatt 1978; Glatzmaier 1983). One of the most spectacular manifestations of the differential rotation in nature is probably the zonal jet flows exhibited by the atmospheres of the major planets. Even more striking is the fact that the zonal jets are virtually constant in both strength and profile, and are highly equatorially symmetric (Ingersoll *et al.* 1981). Differential rotation is likely to be most easily generated through the nonlinear interaction of fluctuating convection eddies with the Reynolds stress in rapidly rotating spherical fluid bodies. The key element involved in generating differential rotation is associated with the phase shift of convection rolls which is emphasized in the models of the mean zonal flows of the major planets (Busse 1976; 1983).

Emphasis throughout this paper is on demonstrating that the combined effects of rotation, spherical curvature and the Prandtl number can create a circumstance in which even weakly nonlinear processes can produce an important consequence: nonlinear interactions of the convection rolls are capable of generating a flow dominated by the differential rotation. In contrast to the earlier numerical studies, focus in this paper is on linear and nonlinear solutions in the parameter region of large Taylor number where the solutions display asymptotic behaviours on the dependence of the Taylor number. Consequently, an extrapolation of our model to rapidly rotating realistic systems becomes feasible. An attempt is also made to show the behaviour of the linear problem at an asymptotically large Taylor number in the hope of providing clues leading to an improvement of the existing analytical linear theories.

In a rapidly rotating spherical system, we expect that velocity deviation from the state of the Proudman–Taylor (PT) two-dimensional condition at the onset of convection would be quite small except in the vicinity of the outer spherical boundary. To illustrate the physical mechanism of the differential rotation generation and to give an insight into the qualitative behaviour of how and why columnar rolls can play a central part in this generation, we assume that the velocity of small-amplitude convection in cylindrical coordinates, (s, ϕ, z), has components,

$$\boldsymbol{u} = \left(-\frac{1}{sT^{\frac{1}{2}}}\frac{\partial p}{\partial \phi}, \frac{1}{T^{\frac{1}{2}}}\frac{\partial p}{\partial s}, u_z \right),$$

where T is the Taylor number (see §2), and p is the deviation of pressure from hydrostatic state in a drifting frame

$$p = A \sin(\pi\zeta) \sin m(\phi - f(\zeta)),$$

and $\zeta = 2(s-s_0)/d$ is the radial distance from the centre of a convection roll scaled by the thickness of the cylindrical convective layer. It is of course oversimplified, but it contains the basic elements of a realistic flow needed for the purpose of illustration. The spiralling properties of the columnar rolls are described by the phase function, $f(\zeta)$, which is primarily associated with the curvature of the boundary and with the value of the Prandtl number as we will discuss further. We will refer to the flow characterized by $\partial f(\zeta)/\partial\zeta \ll 1$ as normal columnar convection (rolls), which was predicted by the theories of Roberts (1968) and Busse (1970*a*); the convection with $\partial f(\zeta)/\partial\zeta \geqslant O(1)$ will be referred to as spiralling columnar convection (rolls). Taking the average of the azimuthal component of the momentum equation (see §2,

equation (2)) over a cylindrical surface, and utilizing the drifting properties of finite-amplitude convection (Zhang & Busse 1987) and the equation of continuity, an equation for the differential rotation can be obtained:

$$\left[2s(u_\phi u_s)+s^2\frac{\partial(u_\phi u_s)}{\partial s}\right]=\left(s\frac{\partial}{\partial s}s\frac{\partial}{\partial s}-1\right)U_\phi,$$

where [ ] represents the integral over a cylindrical surface and the differential rotation is denoted by $U_\phi=[u_\phi]$. Taking into account that the s-derivative is much larger than the z-derivative, $\partial/s\partial s \gg 1$, it yields

$$\frac{\partial U_\phi}{\partial s}\sim[u_\phi u_s]\sim-\int\frac{1}{sT}\frac{\partial p}{\partial\phi}\frac{\partial p}{\partial s}\mathrm{d}\phi.$$

The relationship between the distortion of the columnar rolls and the differential rotation is thus given by

$$\frac{\partial U_\phi}{\partial\zeta}\sim\frac{A^2m^2\pi}{T}\frac{\partial f}{\partial\zeta}\sin^2(\pi\zeta). \tag{1}$$

where $\partial f(\zeta)/\partial\zeta$ is approximately proportional to the inclination angle, η_i, between a stretched convection roll and the radial direction. Several important nonlinear aspects of the problem are captured by this simple illustrative case. It is evident that the Coriolis force cannot sustain the non-vanishing axisymmetric flow $U_\phi(s)$. An equilibrium state is achieved by balancing the Reynolds stress with the viscous forces of the differential rotation. The strength of the differential rotation is approximately proportional to the inclination angle, $\eta_\mathrm{i}\sim\partial f(\zeta)/\partial\zeta$, of a columnar roll. If the phase function $f(\zeta)$ is independent of radial coordinate ζ, that is, $\partial f(\zeta)/\partial\zeta=0$, the differential rotation cannot be maintained by the Reynolds stress. With a substantial tilt of convection rolls, $\eta_\mathrm{i}>45°$, a large-amplitude differential rotation of the order of $U_\phi=O(u_s u_\phi)$ can be generated through nonlinear interactions between the spiralling rolls. The direction of the differential rotation is determined by the sign of $\partial f(\zeta)/\partial\zeta$. Provided that the convection roll spirals progradely, $\partial f(\zeta)/\partial\zeta>0$, U_ϕ will be predominantly eastward in lower latitudes.

In rotating spherical convection systems, it is the fluid properties characterized by the Prandtl number that determine the fundamental features of both thermal instabilities and the corresponding nonlinear convection. Special attention will thus be given to the Prandtl-number-dependence of the problem, which has received very little attention. We shall present the linear and nonlinear results in rotating spherical fluid shells with the parameters in the ranges

$$O(10^8)\leqslant T\leqslant O(10^{12}),\ O(0.1)\leqslant Pr\leqslant 100$$

and $0\leqslant(R-R_\mathrm{c})\leqslant 2R_\mathrm{c}$, where R_c represents the critical Rayleigh number required for the onset of convection, and T is the Taylor number associated with the rate of rotation of the system. Attention is mainly focused on the case of the radius ratio of the spherical shell at $r_\mathrm{i}/r_\mathrm{o}=\eta=0.4$, but the influences of varying η on the pattern of convection will also be discussed. Complicated nonlinear solutions bifurcating supercritically from the spiralling roll instability support the simple and physically illustrative ideas developed in (1). The relationship between the spiralling of convection rolls and the corresponding nonlinear properties of the flow will be particularly emphasized. Though the various applications of the results will not be

emphasized, the new form of instability and its finite-amplitude properties will certainly shed light on a broad class of geophysical and astrophysical problems in which the spherical systems are characterized by moderate Prandtl numbers and are strongly influenced by rotation.

In what follows we first present the mathematical formulation of the problem in §2. In §3 we discuss the instability criteria for the onset of convection at asymptotically large Taylor numbers as a function of the Prandtl number. In §4, the structure of linear convection is illustrated and the physical reason for the occurrence of spiralling columnar convection is discussed. Nonlinear properties of convection are shown in §5. The paper closes with a brief discussion of the main features of our analysis and concluding remarks.

2. Mathematical formulation of the problem

Consider a homogeneous fluid spherical shell of constant thermal diffusivity κ, fluid thermal expansion coefficient α and viscosity ν that is rotating uniformly with a constant angular velocity Ω in the presence of its own gravitational field

$$\boldsymbol{g} = \gamma \boldsymbol{r},$$

and in the absence of external forces. As the qualitative features of convection may not be critically influenced by the choice of the reference state (Chandrasekhar 1961), we have adopted the traditional model (Roberts 1968; Busse 1970*a*; Soward 1977) in which the basic temperature gradient,

$$\nabla T_s = -\beta \boldsymbol{r}$$

is produced by a uniform distribution of heat sources.

Using the thickness of the fluid shell, $d = r_0 - r_i$, as lengthscale, the viscous diffusion time, d^2/ν, as scale of time, and βd^2 as scale of temperature fluctuation of the system, respectively, the Navier–Stokes equation of motion for the velocity, $\boldsymbol{u}$, the heat equation for the temperature deviation, Θ, from the purely conductive state, T_s, can be written as

$$\left(\frac{\partial}{\partial t} + \boldsymbol{u}\cdot\nabla\right)\boldsymbol{u} + \tau \boldsymbol{k}\times\boldsymbol{u} = -\nabla p + R\boldsymbol{r}\Theta + \nabla^2\boldsymbol{u}, \tag{2}$$

$$\nabla\cdot\boldsymbol{u} = 0, \tag{3}$$

$$\left(\nabla^2 - Pr\frac{\partial}{\partial t}\right)\Theta + \boldsymbol{r}\cdot\boldsymbol{u} = Pr\,\boldsymbol{u}\cdot\nabla\Theta, \tag{4}$$

where $\boldsymbol{k}$ is an unit vector parallel to the axis of rotation, and $\boldsymbol{u}$ is the three-dimensional velocity field, (u_s, u_ϕ, u_z), in cylindrical coordinates, and, (u_r, u_θ, u_ϕ), in spherical polar coordinates. The term ∇p represents the force due to the pressure gradient. The non-dimensional parameters in the above equations are the Rayleigh number R, the Prandtl number Pr and the Taylor number T, defined as

$$R = \frac{\alpha\beta\gamma d^6}{\nu\kappa}, \quad Pr = \frac{\nu}{\kappa}, \quad T = \tau^2 = \left(\frac{2\Omega r_0^2}{\nu}\right)^2 (1-\eta)^4.$$

In the frame of the Boussinesq approximation, the velocity field can be written as a sum of poloidal and toroidal vectors

$$\boldsymbol{u} = \nabla\times\nabla\times\boldsymbol{r}v + \nabla\times\boldsymbol{r}w.$$

Making use of this expression and applying $\boldsymbol{r}\cdot\boldsymbol{\nabla}\times$ and $\boldsymbol{r}\cdot\boldsymbol{\nabla}\times\boldsymbol{\nabla}\times$ onto (2), we can derive the three independent governing non-dimensional scalar equations,

$$\left[\left(\nabla^2-\frac{\partial}{\partial t}\right)L_2+\tau\frac{\partial}{\partial\phi}\right]\nabla^2 v+\tau Qw-RL_2\Theta=-\boldsymbol{r}\cdot\boldsymbol{\nabla}\times\boldsymbol{\nabla}\times(\boldsymbol{u}\cdot\boldsymbol{\nabla}\boldsymbol{u}), \tag{5}$$

$$\left[\left(\nabla^2-\frac{\partial}{\partial t}\right)L_2+\tau\frac{\partial}{\partial\phi}\right]w-\tau Qv=\boldsymbol{r}\cdot\boldsymbol{\nabla}\times(\boldsymbol{u}\cdot\boldsymbol{\nabla}\boldsymbol{u}), \tag{6}$$

$$\left(\nabla^2-Pr\frac{\partial}{\partial t}\right)\Theta+L_2 v=Pr\boldsymbol{u}\cdot\boldsymbol{\nabla}\Theta. \tag{7}$$

In spherical polar coordinates (r,θ,ϕ) with polar axis in the direction of rotation $\boldsymbol{k}$, the differential operators, L_2 and Q, are defined as

$$L_2=-r^2\nabla^2+\frac{\partial}{\partial r}r^2\frac{\partial}{\partial r},\quad Q=\boldsymbol{k}\cdot\boldsymbol{\nabla}-\tfrac{1}{2}(L_2\boldsymbol{k}\cdot\boldsymbol{\nabla}+\boldsymbol{k}\cdot\boldsymbol{\nabla}L_2).$$

Equations (5)–(7) must be solved subject to certain conditions on the spherical bounding surfaces. The assumptions of impenetrable, perfectly thermally conducting and stress-free boundaries impose the following boundary conditions at the inner and outer bounding spherical surfaces,

$$v=\Theta=\frac{\partial^2 v}{\partial r^2}=\frac{\partial}{\partial r}\left(\frac{w}{r}\right)=0,$$

at $r_{\mathrm{i}}=\eta/(1-\eta)$ and $r_{\mathrm{o}}=1/(1-\eta)$. The stress-free boundaries are assumed since the nature of the boundaries may have little influences on the leading-order solution in the regime of large Taylor number (Roberts 1965). The frame of reference in which the rigid-body rotation of fluid motions vanishes has been adopted. However, the transformation to the other frame of reference is possible after a nonlinear solution is obtained. Moreover, the same thermal boundary conditions are used in the nonlinear computation because of the small volume of the inner core (see discussions in Zhang & Busse 1989).

With the employment of the Galerkin spectral method in our numerical analysis, the three variables of the equations are represented in terms of complete systems of functions with the radial functions satisfying the boundary conditions,

$$\Theta=\sum_{l,m,n}\Theta_{lmn}\sin n\pi(r-r_{\mathrm{i}})\,Y_l^m(\theta,\phi)\exp\mathrm{i}\omega t+\mathrm{c.c.},$$

$$v=\sum_{l,m,n}v_{lmn}\sin n\pi(r-r_{\mathrm{i}})\,Y_l^m(\theta,\phi)\exp\mathrm{i}\omega t+\mathrm{c.c.},$$

$$w=\sum_{l,m,n}rw_{lmn}\cos n\pi(r-r_{\mathrm{i}})\,Y_l^m(\theta,\phi)\exp\mathrm{i}\omega t+\mathrm{c.c.},$$

where coefficients Θ_{lmn}, v_{lmn} and w_{lmn} are complex and time independent, and c.c. denotes complex conjugate, which should be included in the expansions for nonlinear solutions and excluded for linear solutions. The system possesses an equatorial symmetry that allows separation of the solution of (5)–(7) into two distinct families. The first family selects the spherical harmonics with a symmetry:

$$(u_r,u_\theta,u_\phi)(r,\theta,\phi)=(u_r,-u_\theta,u_\phi)(r,\pi-\theta,\phi),$$

which we shall call the symmetric mode. The other family with the opposite symmetry with respect to the equator will be referred to as the antisymmetric mode.

We shall consider the symmetric mode only for the reason that it represents the physically realized solution (Busse 1970*a*).

3. Onset of thermal instabilities

In determining the onset of convection, all the nonlinear terms in (5)–(7) are neglected as the system deviates slightly from the state of rigid-body rotation. On marginal instability, the requirement that both the real and imaginary parts of the complex determinant of the equation matrix (resulting from the Galerkin procedures) vanish yields two real equations

$$G_{\mathrm{r}}(\omega, R, T, m, Pr) = G_{\mathrm{i}}(\omega, R, T, m, Pr) = 0,$$

for given values of azimuthal wavenumber m, Taylor number T and Prandtl number Pr. Because of the Rossby wave-like character of the instability, ω generally does not vanish. The equations G_{r} and G_{i} can be solved for the values of ω and R by an iteration scheme. The critical mode of instability corresponds to the smallest possible value of the Rayleigh number, R_{c}, with respect to all possible values of azimuthal wavenumber and to all possible modes likely to be excited. The amount of computation involved in determining the critical mode of convection is enormous, particularly for high Taylor numbers. Our attention is confined to the parameter ranges $10^8 \leqslant T \leqslant 10^{12}$ and $O(0.1) \leqslant Pr \leqslant 100.0$. Approximate numerical solutions are obtained by truncating an infinite set of linear homogeneous complex equations with a triangular truncation scheme in which all coefficients with indices satisfying

$$(l-m)+2n > 2N_{\mathrm{t}}+1 \tag{8}$$

are neglected. The resolution of linear solutions described in this paper is sufficient for about 3% accuracy. Some examples of the numerical convergence of linear solutions are presented in table 1. To give an impression of the resolution, for instance, the highest degree, l_{h}, of the spherical harmonics $Y_l^m(\theta, \phi)$ included at the truncation level $N_{\mathrm{t}} = 22$ for $T = 10^{12}$, $m = 73$ and $Pr = 10$ is $l_{\mathrm{h}} = 118$. Moreover, the associated patterns of convection at different levels of truncation display almost identical forms.

We begin our discussions of the linear results with a brief discussion of several previous studies. A detailed discussion about the existing theories can be found, for example, in a comprehensive review article by Fearn, Roberts & Soward (1988). Theoretical treatments of the linear-instability problem in a full sphere at large T limit were carried out by Roberts (1968) and Busse (1970*a*). An important development of the linear theories has been made by Soward (1977) who extended the linear stability analysis to a weakly nonlinear regime to reveal the radial structure of convection columns. Moreover, by applying the no-slip boundary conditions he was able to investigate effects of the Ekman suction into and out of spherical boundary layers, which may have controlling influences on large-scale azimuthal flows. Another important extension of the theories is concerned with the influences of magnetic fields on the thermal instability (Fearn 1979*a*, *b*), which will not be pursued here.

The essential elements in all the earlier theoretical studies involve three different scales: the short azimuthal lengthscale of the convection rolls, $r_{\mathrm{o}} T^{-\frac{1}{6}}$, the medium radial lengthscale, $r_{\mathrm{o}} T^{-\frac{1}{3}}$, and the long lengthscale in the direction of the rotation axis, r_{o}. Consequently, the mathematical problem of the linear convection is considerably simplified by assuming that the azimuthal derivative, $\partial/\partial\phi$, dominates over the axial and the radial derivatives; the complex linear problem associated with

N_t	T	R_c	m	ω
12	10^{10}	7.05×10^6	30	−99.8
13	10^{10}	7.06×10^6	30	−98.9
14	10^{10}	7.07×10^6	30	−98.8
15	10^{10}	7.07×10^6	30	−98.8
20	10^{12}	1.513×10^6	73	−490.5
21	10^{12}	1.475×10^8	73	−472.3
22	10^{12}	1.456×10^8	73	−458.4
23	10^{12}	1.445×10^8	73	−446.1

TABLE 1. Examples of the convergence behaviour of the critical parameters at the onset of convection with increasing truncation parameter N_t at $Pr = 10$

partial differential equations is reduced to local stability analysis in connection with ordinary differential equations. Such a numerical system with a second-order differential equation describing the asymptotic dependence of the critical parameters, R_c, m_c and ω_c on the Taylor number T,

$$R_c = C_R T^{\frac{2}{3}}, \quad m_c = C_m T^{\frac{1}{6}}, \quad \omega_c = C_\omega T^{\frac{1}{3}}$$

was first derived by Roberts (1968), where the coefficients are a function of the Prandtl number. But the anti-symmetric mode of convection was considered. The physically realizable asymptotic relations with the correct equatorial symmetry were obtained by Busse (1970*a*). By taking the curvature effect of boundaries as a perturbation, he was able to obtain the critical coefficients at asymptotically large T given by the following analytic expressions

$$C_R = 0.8021\left(\frac{Pr}{1+Pr}\right)^{\frac{4}{3}}, \tag{9}$$

$$C_\omega = -1.204\left(\frac{1}{Pr(1+Pr)^2}\right)^{\frac{1}{3}}, \tag{10}$$

$$C_m = 0.5470\left(\frac{Pr}{1+Pr}\right)^{\frac{1}{3}}, \tag{11}$$

in which we have taken into account the different scale used in his analysis.

The radial structure of convective instabilities left undetermined in the above analysis was partly resolved by the Soward's (1977) weakly nonlinear instability theory, where the source of difficulties for determining the radial structure in the linear theories of Roberts and Busse was also traced. As a higher approximation to Busse's theories, the finite change of the boundary curvature across the convection layer of the medium lengthscale, $T^{-\frac{1}{6}}$, was taken into account in Soward's theory. It is interesting to note that the possibility that convection rolls may have a prograde phase shift is implicit in his results, in which the quantity $B \sim \partial\tilde{s}/\partial\tilde{\omega}$ (equation (4.14*b*), Soward 1977), equivalent to $\partial f(\zeta)/\partial\zeta$, is positive. Of particular interest in his results is the fact that the steady or Rossby wave-type convection solutions with the critical Rayleigh number close to the value determined by Busse (1970*a*) do not exist. Consequently, the critical Rayleigh number for the onset of convection cannot be predicted on the basis of the Roberts–Busse local linear theories.

The critical coefficients, C_R, C_ω and C_m, estimated from our numerical solutions up to the Taylor number $T = O(10^{12})$, and evaluated from (9)–(10), are displayed in

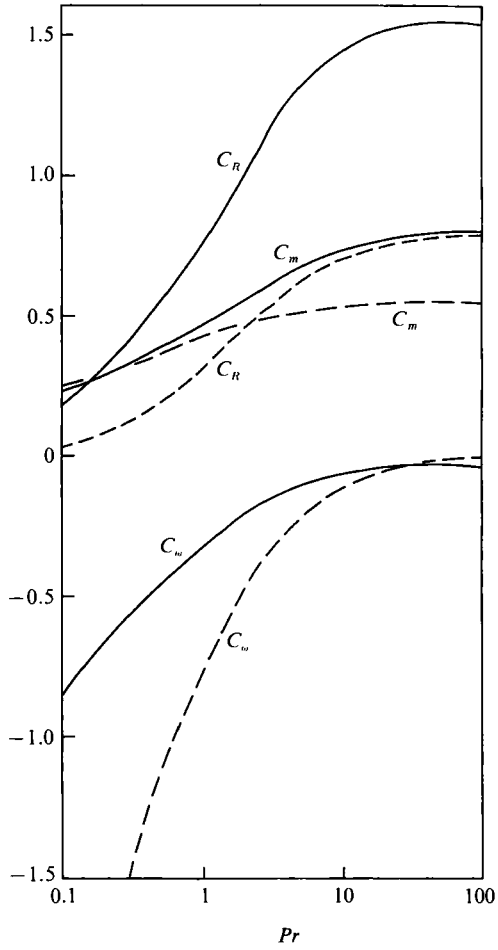

FIGURE 1. The critical coefficients plotted against the Prandtl number. The dashed curves correspond to (9)–(11) and the solid curves are obtained from numerical analysis.

C	$T = 10^8$	$T = 10^9$	$T = 10^{10}$	$T = 10^{11}$	$T = 10^{12}$
$R_c/T^{2/3}$	1.61	1.56	1.52	1.48	1.45
$-\omega_c/T^{1/3}$	0.043	0.044	0.046	0.045	0.044
$m_c/T^{1/6}$	0.65	0.70	0.65	0.71	0.73

TABLE 2. Examples of the convergence behaviour of the critical parameters at the onset of convection with increasing Taylor number

figure 1. Table 2 shows an example of the convergence behaviour of the dependence of the critical coefficients as a function of the Taylor number for $Pr = 10$. Several interesting points have emerged from the table and the instability curves. Evidently, the power-law dependence, $R_c \sim T^{\frac{2}{3}}$, $\omega_c \sim T^{\frac{1}{3}}$ and $m_c \sim T^{\frac{1}{6}}$, at the onset of convection is borne out at large T; the parameter region with the asymptotically large T behaviour is apparently reached by our numerical analysis with about 5% accuracy. However, the critical Rayleigh number required for the instability of convection is much underestimated by (9), while the frequency of oscillation is much

overestimated, particularly for small Prandtl numbers. That the coefficient of the critical Rayleigh number R_c significantly exceeds the value of the Robert–Busse local theory appears to support the suggestion made by Soward (1977). It is also of importance to note that the ratio of the numerical estimate to the theoretical value varies quite substantially as a function of Pr. While the critical wavenumber of the theories and of the numerical results is nearly the same for the Prandtl number $Pr \leqslant 1$ the difference increases sharply with increasing Prandtl number. It is also interesting to note that both the theories and the numerical results show a tendency of asymptotically large Pr dependence for $Pr \geqslant 10$.

Another key parameter in discussing wave phenomena is the group wave speed, defined as

$$C_g = \frac{\partial \omega}{\partial m},$$

in which the sign of C_g gives rise to the direction of propagation of wave energy. Our numerical results indicate that the wave energy propagates westward ($C_g < 0$) when the Prandtl number $Pr \leqslant O(1)$, consistent with the existing theories, but the propagation of wave energy ($C_g > 0$) becomes eastward when the Prandtl number $Pr \geqslant O(10)$. The critical Prandtl number at which the Rossby waves stop propagating energy ($C_g = 0$) seems to be around $Pr = 5$. This discrepancy is perhaps a result of the fact that the position of convection is strongly dependent on the Prandtl number (see figure 3).

To search for the reason for the discrepancy between our analysis and the theories, it is natural first to test the assumption of the theories on the different scales of convection rolls. The question of whether or not the radial scale of the columnar rolls is much larger than the azimuthal scale can be answered by comparing the variation of $\boldsymbol{u}$ as a function of $s-s_i$, where $s_i = r_i$, at fixed values of z_0 and ϕ_0, with the variation of $\boldsymbol{u}$ as a function of $s_0(\phi-\phi_0)$ at fixed values of z_0 and s_0. Such comparisons at the equatorial plane are displayed in figure 2 for three different Prandtl numbers, namely $Pr = 0.1$, 1.0 and 10.0, in which the s-dependence of u_s and u_ϕ is denoted by solid lines and the $s_0(\phi-\phi_0)$-dependence is represented by dashed lines. As a result of the equatorial symmetry condition, flows are not allowed to cross the equatorial plane, that is, $u_z = 0$ at the equatorial plane. At a moderately small Prandtl number $Pr = 0.1$ (figure 2*a*), the amplitude of velocity peaks at about $s-s_i = 0.35$ and decreases apparently algebraically away from the peak. At the radial distance, $s_0-s_i \approx 0.35\,(\theta \approx 37°)$, the radial wavelength, λ_s, measured between two successive peaks of u_s or u_ϕ is about 0.18 which is eventually smaller than the azimuthal wavelength $\lambda_m = 0.29$. Apparently, the radial wavelength λ_s remains nearly constant, reflecting the fact that it may result from the spiralling of the rolls. At the second peak, $s_0-s_i = 0.63$, the azimuthal wavelength λ_m becomes nearly equal to $2\lambda_s$. It appears that there are only two different scales for the convection: the short lengthscale of convection roll in both azimuthal and radial directions, and the long lengthscale in the direction of rotation axis,

$$\frac{\partial}{\partial \phi} \approx \frac{\partial}{\partial s} \gg \frac{\partial}{\partial z}.$$

As Pr is increased to $Pr \geqslant 1.0$, however, three different scales start to emerge (figures 2*b*, 2*c*):

$$\frac{\partial}{\partial \phi} > \frac{\partial}{\partial s} \gg \frac{\partial}{\partial z}.$$

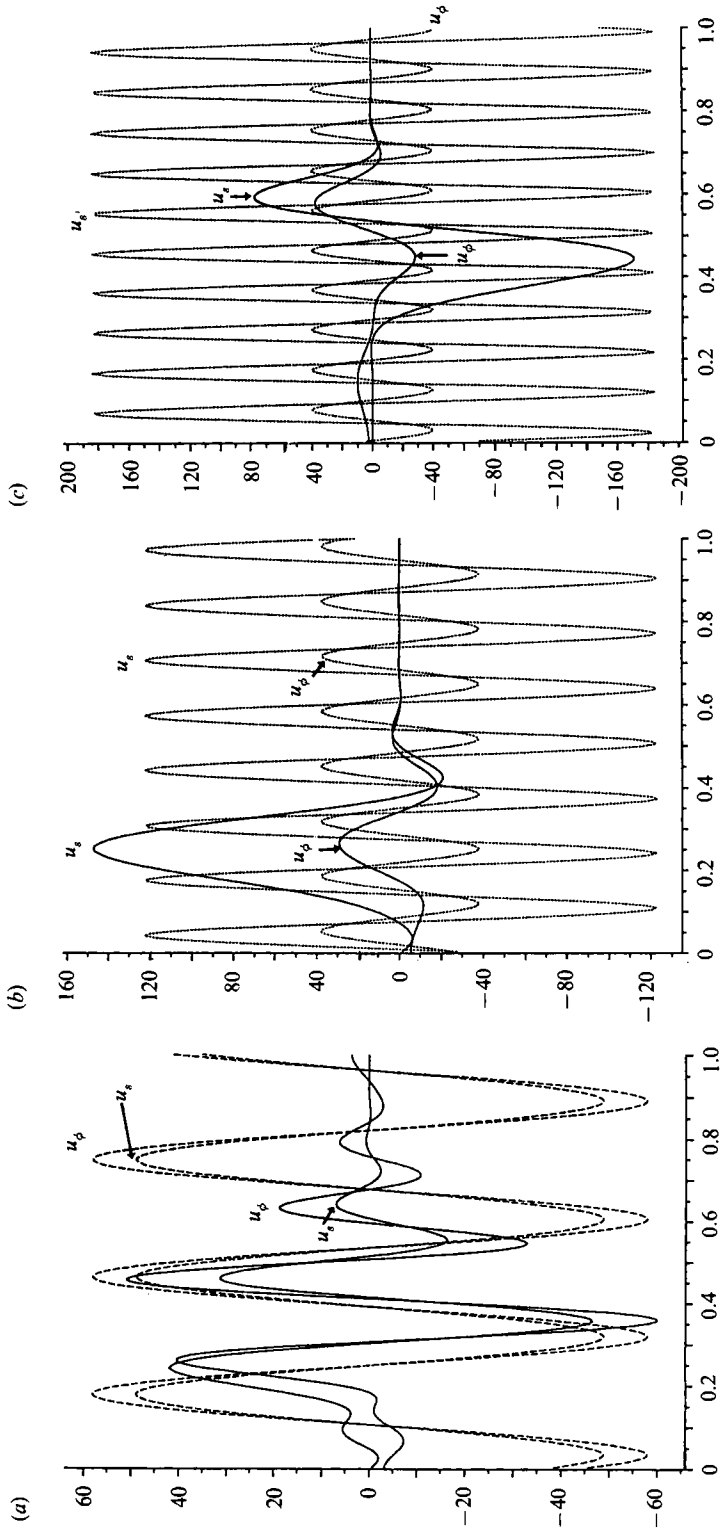

FIGURE 2. Velocity components, u_s and u_ϕ plotted as a function of $s-s_1$ (solid lines) for $\phi_0 = 0$, and as a function of $s_0(\phi-\phi_0)$ (broken lines) for $\phi_0 = 0$, where s_0 is the distance from the axis of rotation at which convection is mainly concentrated. The parameters are (*a*) $Pr = 0.1$, (*b*) $Pr = 1$ and (*c*) $Pr = 10$ at $T = 10^{11}$.

From the condition $\nabla \cdot \boldsymbol{u} = 0$, which gives rise to

$$\frac{u_s}{u_\phi} \approx \frac{\lambda_s}{\lambda_m},$$

it is expected that the dependence of the scales on the Prandtl number should also be reflected by the typical ratio of the radial and the azimuthal components of velocity, u_s/u_ϕ. For $Pr = 0.1$, the amplitudes of u_s and u_ϕ is comparable with the typical value of u_s/u_ϕ slightly less than 1. As Pr is increased (see figure 2), u_s/u_ϕ increases rapidly in response to the changing of the scales of the roll. In order to keep the relatively longer radial scale, the amplitude of u_s needs to greatly exceed that of u_ϕ. Another important feature in figure 2 is the position of the concentration of convection which also shows a strong dependence on the Prandtl number. In short, the discrepancy between our linear results and the earlier analyses is probably a consequence of an assumption of the theories: there exist three different scales of the convection roll regardless of the size of the Prandtl number.

4. Structure of columnar convection

It is the PT theorem in conjunction with the controlling influences exerted by boundary geometry that provide the key for understanding the structure of convection in rapidly rotating fluid systems. The PT theorem states that a steady and slow motion in the absence of viscous and magnetic forces satisfies the following vorticity equation

$$(\boldsymbol{k} \cdot \nabla)\, \boldsymbol{u} = 0. \tag{12}$$

It follows that the flow satisfying (12), the so-called geostrophic flow, is therefore independent of the coordinate parallel to the axis of rotation, and the pressure performs as a stream function for the two-dimensional flow. However, the realization of a convective flow obeying the PT theorem depends upon the geometry of the bounding surfaces of a fluid container on which

$$u_z + \chi(s)\, u_s = 0,$$

must be satisfied, where χ is associated with the geometry of the fluid container, assumed to be axisymmetric. In a rotating annulus with parallel top and bottom boundaries, $\chi = 0$, two-dimensional convection can be realized except in the thin Ekman layers. In a rotating annulus with constant inclined top and bottom boundaries, $\partial\chi/\partial s = 0$, convection without violating the PT theorem cannot occur. The resulting convection is in the form of nearly two-dimensional rolls aligned parallel to the axis of rotation, and the rolls drift in the azimuthal direction with phase speed proportional to the slope of the boundaries, χ. With an addition of weak curvature on the boundaries, $\partial\chi/\partial s = \epsilon$, where ϵ is a small parameter, the phase of the convection roll shifts slightly in the azimuthal direction depending on the sign of ϵ (Busse 1983). In a rotating spherical system, the effects of spherical boundary curvature described by

$$\partial\chi/\partial s = \frac{1}{r_0(1-(s/r_0)^2)^{\frac{3}{2}}},$$

together with the strong influences of the Coriolis force play a key role in causing a drastic distortion of convection rolls in the form of prograde spiral.

A typical structure of the spiralling columnar convection is illustrated in figure

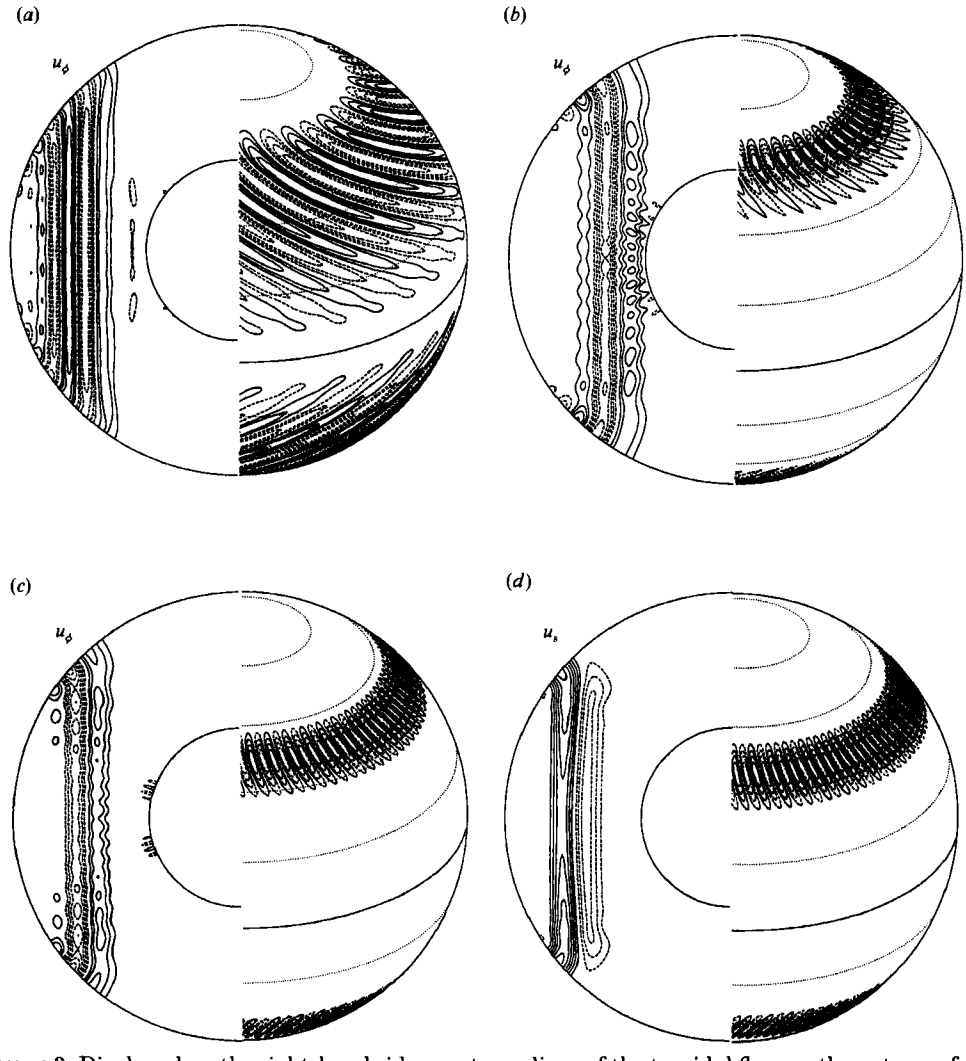

FIGURE 3. Displayed on the right-hand side are streamlines of the toroidal flow on the outer surface of the fluid shell. On the left-hand side of (*a*), (*b*) and (*c*) are contours of u_ϕ in a meridian plane, while contours of u_s are shown in (*d*). The respective parameters are $Pr = 0.1$, $Pr = 1$, $Pr = 10$ and $Pr = 100$ for $T = 10^{11}$. It should be noted that the pattern as a whole drifts with a phase speed $c = -\omega/m$.

3 (*a*) for $T = 10^{11}$ and $Pr = 0.1$. Displayed are streamlines for the toroidal component of velocity on the outer surface of the shell (on the right-hand side) and contours of the azimuthal component, u_ϕ, at a meridian cross-section (on the left-hand side). Other components, such as radial velocity display similar spiral structure and are therefore not shown here. Since the pattern of flows is presented in a frame of reference moving azimuthally with the phase speed of the convection rolls, the profile appears steady. Fluid rising near a latitude 60° is convected down at substantially lower latitudes in the neighbourhood of the equator. At the same time, in attempting to satisfy the two-dimensional constraint, the variation of flows is minimized in the direction of z, as clearly shown by the contours of u_ϕ. The elongated and prograde spiralling roll spans an azimuthal distance of about five wavelengths, while the inclination angle, η_1, is about 50° if it is evaluated approximately by

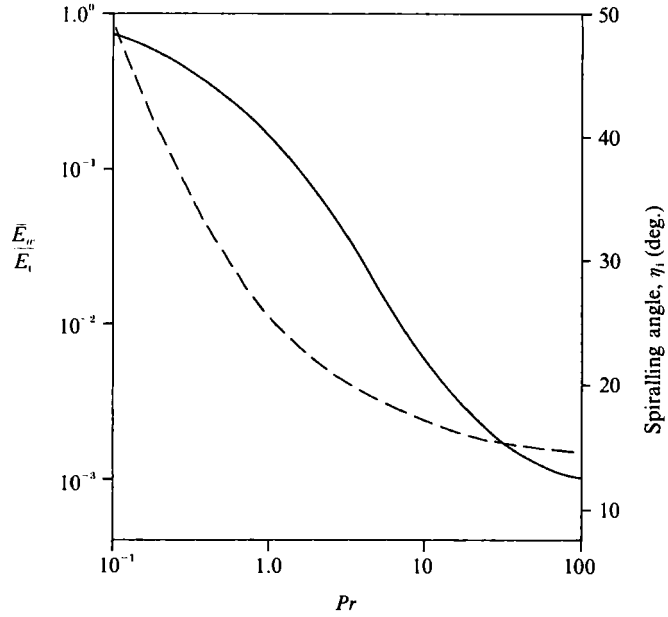

FIGURE 4. ——, $\bar{E}_w/E_t$ at $(R-R_c)/R_c \approx 0.1$ and ---, the estimated spiralling angle plotted as a function of the Prandtl number.

$\eta_i = \tan^{-1}(\lambda_\phi/\lambda_s)$ at $s_0/r_o = 0.5$. There are no clear centres of the vortices as flows move all the way from the region near the equator up to a latitude corresponding to the cylinder attached to the inner boundary equator. As the Prandtl number decreases further, the effects of the spiralling become even more pronounced: the elongated rolls, for example at $Pr = 0.05$, extend in the manner of prograde spiralling from near a latitude 60° all the way to the equator with a large inclination angle. One consequence of the spiralling is that the difference between the scales of the azimuthal and radial direction become negligibly small, as is evident in the contours of u_ϕ. A second consequence, much more significantly, is that the spiralling causes a close correlation between different components of convection ($\int u_s u_\phi \, d\phi \neq 0$).

The fundamental features of the flow structure, however, change markedly with increasing Prandtl number. This change is primarily demonstrated in two ways. Firstly, the magnitude of the spiralling angle decreases sharply with increasing Prandtl number. As Pr is increased from $Pr = O(0.1)$ to asymptotically large values, the spiralling angle η_i (figure 4, dashed curve) decreases accordingly from about 50° to 15°. This variation is also clearly illustrated in figure 3, where toroidal streamlines for three other Prandtl numbers, namely $Pr = 1, 10$ and 100, are displayed. While the spiralling at unit Prandtl number is still substantial, it becomes insignificant in the case of $Pr \geqslant O(10)$, where viscous dissipations are dominant. It appears that the changeover from a normal columnar roll without substantial distortion to spiralling columnar convection is smooth and gradual. Radical changes of convection mode, however, occur when the angle η_i approaches 45°, which is indicative of the vanishing distinction between the radial and azimuthal scale of the roll. Another important feature is concerned with the position of convection concentration, characterized by the critical latitude at which a cylindrical convection annulus coaxial with the axis of rotation meets the outer surface. Again the critical co-latitude of convection is strongly dependent on Pr (see also figure 2) and shifts from about $\theta_c = 35°$ for $Pr = 1$ to approximately $\theta_c = 45°$ for asymptotically large Prandtl numbers. Finally,

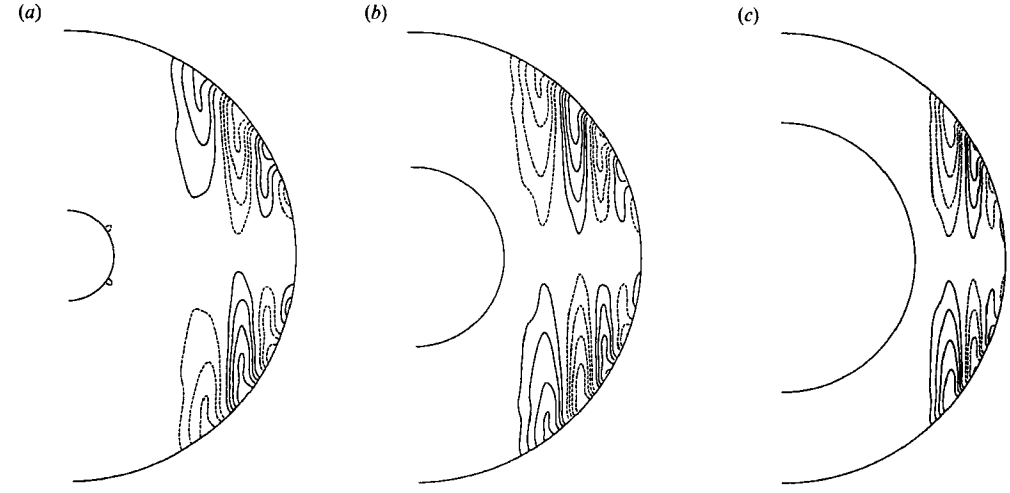

FIGURE 5. Contours of u_z in a meridian plane at $\phi = 0$ shown for (a) $\eta = 0.2$, $T = 5 \times 10^9$, $m = 10$, (b) $\eta = 0.4$, $T = 5 \times 10^9$, $m = 10$, and for (c) for $\eta = 0.6$, $T = 10^9$, $m = 18$ at $Pr = 0.1$. The solid contours indicate northward motion and the dashed contours represent southward motion.

it is worth remarking that the convection rolls observed experimentally (Carrigan & Busse 1983; Chamberlain & Carrigan 1986) with the Prandtl number $Pr \approx 7$ also display a weak but clearly noticeable feature of the spiralling.

The combined effects of the strong Coriolis forces, the boundary of spherical geometry and weak viscous dissipations are responsible for the occurrence of the spiralling columnar convection. While the strong influences of rotation cause the preferred nearly two-dimensional columnar motions, the z-dimension of the column varies continuously as a function of the radial distance. The column of fluid is forced to change its z-dimension as it approaches or moves away from the axis of rotation. That the radial flow must vanish on the outer spherical boundary therefore eventually controls the form of convection; the induced vorticity arising from the z-dimension change of columnar fluid gives rise to the Rossby wave character of convection. It is important to note that the phase speed of the Rossby-type wave is approximately proportional to the inclination of the boundary, and thus increases rapidly, $\partial\chi/\partial s \gg 1$, in the case of spherical geometry as the column of fluid moves toward equator. Consequently, the columnar convection roll in a spherical container is forced to spiral progradely. If the viscous dissipations, measured by the size of the Prandtl number, are not large enough to break it up, it can extend spirally from middle latitudes to the equatorial region and elongate enormously in the azimuthal direction. But the shorter radial scale associated with the spiralling is likely to enhance the thermal diffusion without promoting the action of convection. This may provide an explanation of why the critical Rayleigh number R_c is much higher in comparison with the prediction on the basis of the normal columnar roll.

Influences of the inner core on the spiralling mode are only secondary compared to the effects produced by the Prandtl number. We have carried out the calculation on solutions with different parameters η in an effort to understand the key mechanism of the spiralling columnar convection. Recalling that the problem is scaled by the thickness of the shell, we would expect the value of the critical azimuthal wavenumber to be larger for the thinner shell, and smaller for the thicker shell. Figure 5 depicts contours of u_z at $\eta = 0.2$, 0.4 and 0.6 illustrating the influences of different aspect ratios of the shell on the spiralling properties of the rolls. When

the inner core radius is less than $0.5r_o$, the convection rolls extend spirally from about 60° latitude to lower latitudes and, apparently, the pattern of convection at $\eta = 0.2$ is almost identical to that at $\eta = 0.4$. For $\eta = 0.6$ with $m_c = 18$, the highest latitude reached by the convection corresponds to the latitude at which the cylinder tangential to the inner boundary equator cuts the outer spherical surface (see also Busse & Coung 1977). Since it is a combination of the vastly different phase speed at different latitudes and the effects of lower Prandtl number that markedly distorts the normal convection roll, this distortion will certainly diminish as $\chi(s)$ approaches its asymptotic value in the equatorial region for the limit of a thin spherical shell.

There are no indications of the fundamental change of the roll structure (figure 2) with a further increase of Taylor number. As T increases, though, the lowest latitude that convection can reach becomes higher, owing largely to the larger dissipation of the narrower rolls associated with a larger critical wavenumber. It is also expected that the radial extent of the roll is likely to decrease toward zero as T becomes infinitely large at fixed Pr. However, the basic features such as inclination angle, η_1, and the azimuthal extent of a spiralling roll in terms of the azimuthal wavelength remain unchanged. It seems highly unlikely that these main features will be changed at even higher Taylor numbers.

5. Finite-amplitude properties of spiralling columnar convection

To appreciate that the fluid properties characterized by the Prandtl number play a critical roll in the problem of rotating spherical convection, and to capture the fundamental physical processes associated with the spiralling rolls, further calculation into the nonlinear regime is necessary. This requires the inclusion of all the nonlinear terms neglected in the calculation for the onset of convection, and is a formidable task at such high Taylor numbers owing largely to the rapidly increasing demand on computer hardware. It is for this reason that the range of the parameters which can be investigated is severely limited. However, from the linear results described, we anticipate that the corresponding finite-amplitude solutions depend smoothly on the parameters of the problem. Our attention has therefore been restricted to the cases of $T = O(10^{10})$ with $Pr = 0.1, 1, 10$ and 100. Because the modes associated with the higher harmonics of $m \geqslant 2m_c$ require much larger R in order to be excited and the nonlinear transfer into these higher harmonics is very limited owing to the higher dissipation of large wavenumbers, the higher harmonics related to the azimuthal wavenumber $m \geqslant 2m_c$ (which are, for example, $m \geqslant 32$ for $Pr = 1.0$) are neglected for the range of the Rayleigh number $R < 2R_c$ in our nonlinear calculation. By choosing the parameter of truncation $N_t = 12$, at which the corresponding linear solutions demonstrate satisfactory accuracy (see table 1), fairly accurate finite-amplitude solutions can be obtained for the mildly supercritical Rayleigh number.

General characteristics of finite-amplitude convection can be described by the global properties of a flow such as the kinetic energy density of different components of velocity

$$\bar{E}_w = \langle (\nabla \times \boldsymbol{r}\bar{w})^2 \rangle, \quad \tilde{E}_w = \langle (\nabla \times \mathrm{r}\tilde{w})^2 \rangle, \tag{13}$$

$$\bar{E}_v = \langle (\nabla \times \nabla \times \boldsymbol{r}\bar{v})^2 \rangle, \quad \tilde{E}_v = \langle (\nabla \times \nabla \times \boldsymbol{r}\tilde{v})^2 \rangle, \tag{14}$$

where the over bar indicates the axisymmetric components of flow and the tilde denotes the non-axisymmetric components. The symbol $\langle\ \rangle$ represents the average over the spherical fluid shell. Because of the drifting property of finite-amplitude

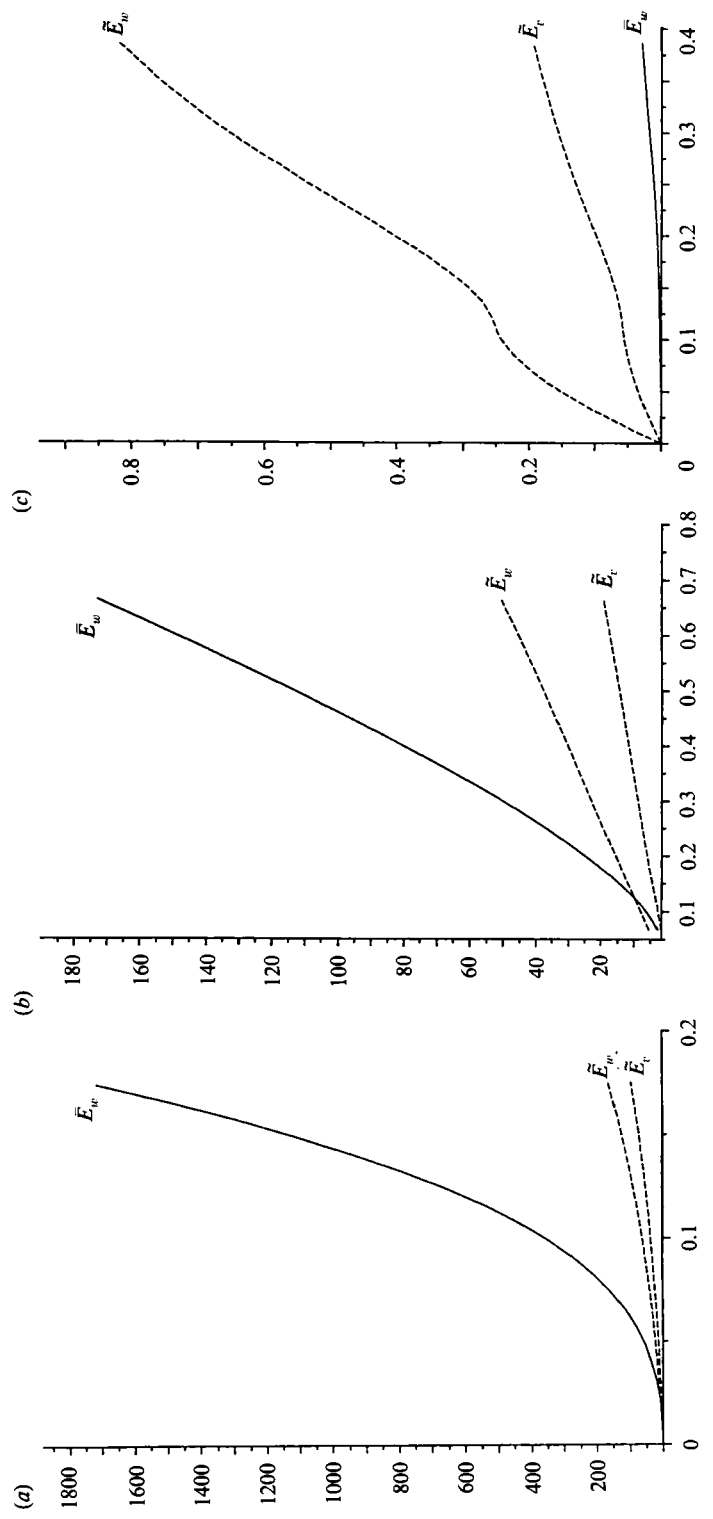

FIGURE 6. Kinetic energies of various components shown as a function of $(R-R_c)/R_c$ for (*a*) $Pr = 0.1$, $T = 5 \times 10^9$, (*b*) $Pr = 1$, $T = 10^{10}$ and (*c*) $Pr = 10$, $T = 10^{10}$. ——, kinetic energy of the differential rotation.

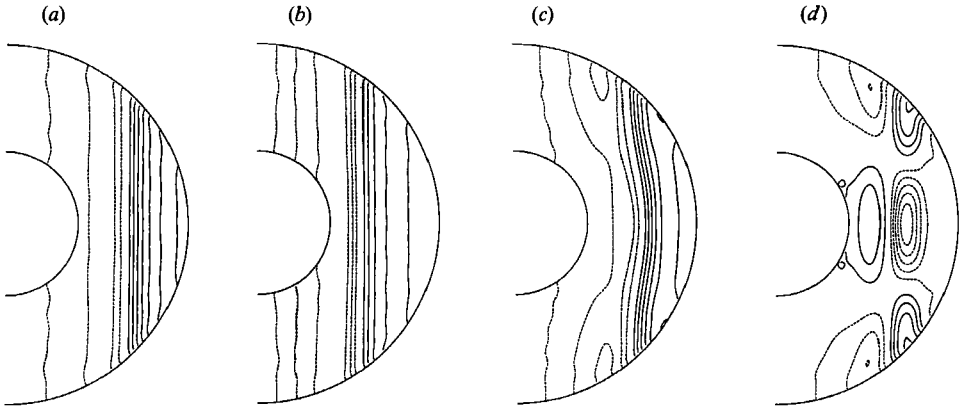

FIGURE 7. Contours of the different rotation U_ϕ, in a meridian plane are shown at four different Prandtl numbers, namely $Pr =$ (*a*) 0.1, (*b*) 1, (*c*) 10 and (*d*) 100, for $(R-R_c)/R_c \approx 0.1$. ——, eastward motion, ---, westward motion and the contour interval is constant.

solutions, not only the axisymmetric components but also the average non-axisymmetric quantities are independent of time. It is convenient to characterize the basic features of a flow by introducing the ratio of the kinetic energy of the mean zonal flow U_ϕ to the total energy E_t,

$$\frac{\bar{E}_w}{E_t} = \frac{\langle U_\phi^2 \rangle}{\langle \boldsymbol{u}^2 \rangle}.$$

The dependence of this ratio on the Prandtl number is plotted in figure 4 (solid line) at a particular value of $(R-R_c)/R_c \approx 0.1$ for $T = O(10^{10})$. About 40 nonlinear solutions of the complete equations are obtained in the range $0 < (R-R_c) < 2R_c$ for every Prandtl number. The energy spectrum for three different Prandtl numbers is displayed in figure 6 as a function of $(R-R_c)/R_c$. The most remarkable feature is that the amplitude of the mean zonal flow shows again a strong dependence on the fluid properties characterized by the Prandtl number. It is quite striking that $\bar{E}_w/E_t$ varies from about 90 % to much less than 1 %. As Pr increases from 0.1 to an asymptotically large value, the characteristic of the finite-amplitude convection changes accordingly from the nearly axisymmetric flow to the regular columnar rolls with very weak axisymmetric components. The finite amplitude convection bifurcating from the spiralling columnar mode is primarily dominated by the component of axisymmetric azimuthal flows at the supercriticality of the order of $(R-R_c)/R_c = O(0.1)$, although non-axisymmetric motions are preferred at the onset of convection. For moderately large Prandtl numbers, by contrast, nonlinear interactions of the rolls are much less important, and the resulting finite-amplitude convection is primarily dominated by the non-axisymmetric components of flows. However, the kinetic energy related to the meridional circulation, $\bar{E}_v$, is severely suppressed by the constraint of rotation irrespective of the Prandtl number, and is too small to be shown in figure 6.

Further impressions of the finite-amplitude properties can be gained from the pattern of axisymmetric flows resulting from the nonlinearity. The profiles of the differential rotation for four different Prandtl numbers, namely, $Pr = 0.1$, 1.0, 10, 100, are depicted in figure 7 at $(R-R_c)/R_c = O(0.1)$. These profiles change very little in the range of the parameter $(R-R_c) < 2R_c$ considered in this paper. For moderate Prandtl numbers, the finite-amplitude convection is composed of the dominant

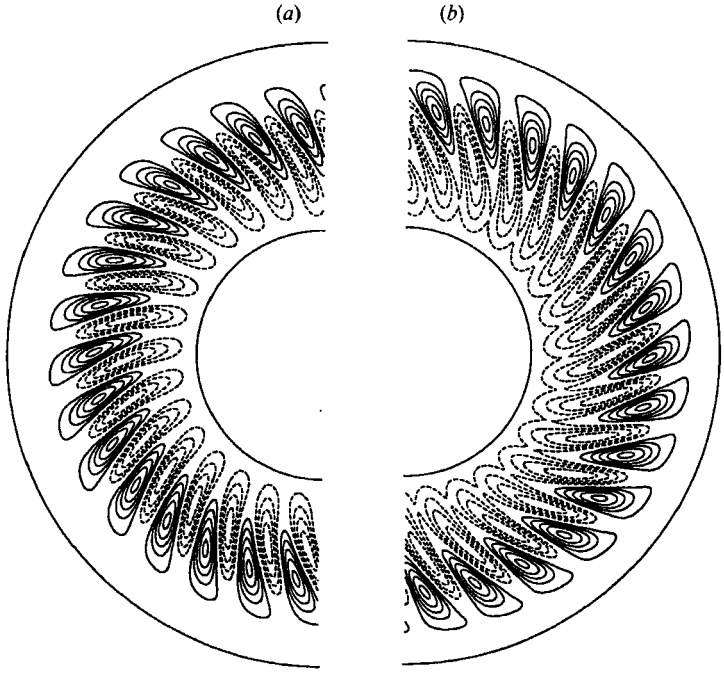

FIGURE 8. Contours the temperature field Θ at the equatorial plane for, (a) $(R-R_c)/R_c = 0.1$ and (b) $(R-R_c)/R_c = 0.3$ for $Pr = 10$ and $T = 10^{10}$.

differential rotation (figure 7a) with weakly superimposed drifting spiralling rolls (figure 3a). The strongest zonal shear apparently occurs at the maximum of the spiralling angle, about 45° latitude. A remarkable feature of the mean zonal flows for $Pr \leqslant O(1)$ is the nearly z-independent structure. In the limit of small Prandtl numbers, the advection of temperature becomes unimportant in comparison with the advection of momentum. The value of the contour interval, $\Delta\Theta_0$, for the corresponding axisymmetric temperature in figure 7(a) is about 0.0013, which gives rise to the mean flow originated from the thermal wind mechanism,

$$T^{\frac{1}{2}}\partial u^t/\partial z \sim Rr \times \nabla\Theta,$$

of the order of $U^t_\phi \approx R\Delta\Theta_0/T^{\frac{1}{2}} \approx 0.01$. This is negligible in comparison with the amplitude of the zonal flow in figure 7(a). However, the character of finite-amplitude convection with moderately large Pr differs in a fundamental way from that of lower Pr. The nonlinear flow with moderately large Pr is primarily dominated by regular columnar rolls (figure 3c, 3d) with a superimposed weak but strongly z-dependent mean flow (figure 7c, d), as we may expect from the linear results. The corresponding differential rotation is primarily generated by the thermal wind mechanism. As a consequence of strong temperature advection, the spherically symmetric basic state is modified by a fairly large axisymmetric component of the temperature field, $\Theta_{m=0}$. In fact, a two-layer structure of Θ, as shown in figure 8, is formed as a result of the modulation.

For the possible application of the nonlinear solutions to zonal flows observed on the top of the atmospheres of the major planets, the axisymmetric zonal velocity $U_\phi(90-\theta)$, and the axisymmetric heat flux, $H = -\partial\Theta_0(90-\theta)/\partial r$, on the outer spherical surface are shown as a function of latitude for four different Rayleigh

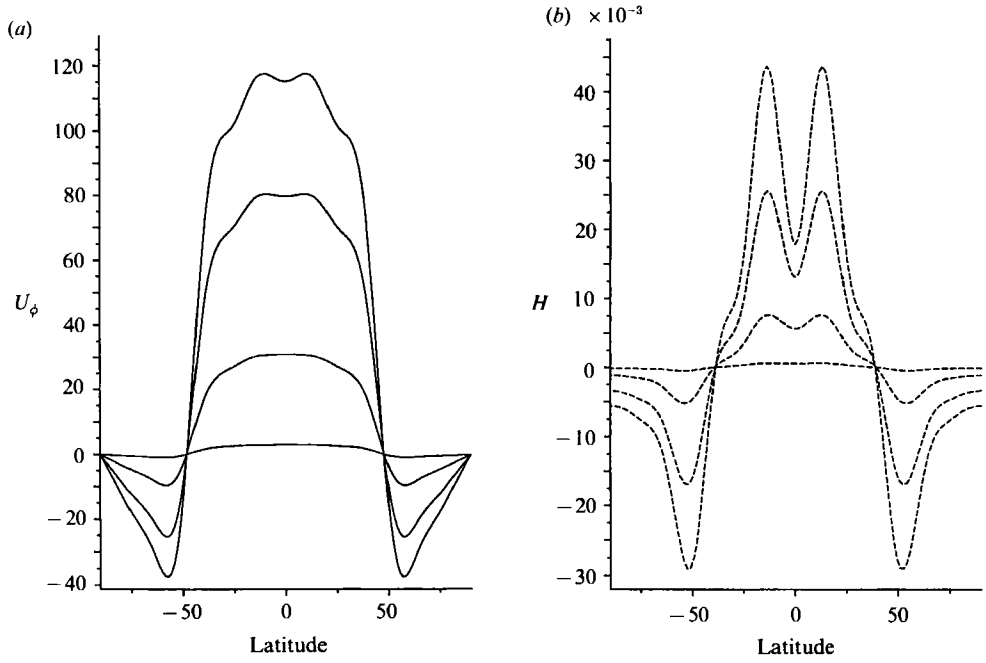

FIGURE 9. (*a*) The axisymmetric velocity component, U_ϕ, and (*b*) the azimuthally averaged heat flux, $-\partial\Theta_0/\partial r$ shown as a function of latitude for the Rayleigh number $(R-R_c)/R_c = 0.008, 0.065, 0.133, 0.175$, successively, at $Pr = 0.1$ and $T = 5\times10^9$ on the outer surface of the fluid shell.

numbers in figure 9(*a*, *b*). A comparison of figures 9(*a*) and 9(*b*) shows a surprising correlation between the latitudinal dependence of axisymmetric heat flux and the mean zonal flow. Both the profiles show the minimum at the equator. The outward mean heat flux peaks near 13° latitude while the zonal velocity reaches a maximum near 10°. The equatorial minimum of zonal flows and heat flux can be explained as arising from the finite latitude at which the outer cylindrical surface of spiralling columns cuts the outer spherical surface. It is of some interest to note that the feedback from the differential rotation to the spiralling columnar rolls appears to be small, as the structure of the non-axisymmetric components shows only a slight change from the onset of convection.

The essential differences between finite-amplitude solutions of different Prandtl numbers can be most easily explained in terms of the Reynolds stress that is closely associated with the form of convection rolls. The huge axisymmetric zonal flows with a geostrophic character for moderate Prandtl numbers can be explained as being due almost entirely to nonlinear interactions of the spiralling rolls as discussed in § 1. Our nonlinear results strongly suggest that the geostrophic character of the mean flow, $\partial U_\phi/\partial z \approx 0$, is not because a geostrophic mode can be most easily excited in a rapidly rotting fluid system, but because it is generated by strong nonlinear interactions of the nearly two-dimensional spiralling columnar rolls. This argument is supported by the transition, with increasing Prandtl number, from the geostrophic-type to the strongly z-dependent, which is clearly illustrated in figure 7. As can be inferred from (1), the amplitude of the mean zonal flow may exceed that of either the non-axisymmetric poloidal or toroidal component of the flow, provided that the degree of spiralling is large enough to cause a close correlation between u_s and u_ϕ which results in a strong momentum advection and produces large Reynolds stresses. Such

nonlinear interactions between the spirally stretched rolls are, with little doubt, responsible for the generation of the huge axisymmetric zonal flow. As zonal shears arising from the differential rotation increase further at higher R, the corresponding distortion of the spiralling columnar rolls is highly likely to limit the growth of the amplitude of the zonal flow. It seems feasible that an elongated spiralling roll is split into several columnar rolls as required by Busse's model of Jupiter's mean zonal flows (1983). Instabilities associated with the strong zonal shear and the likely structure of more complicated flows can be investigated by stability analysis with respect to the nonlinear solution described. However, this type of investigation involving the higher bifurcation of nonlinear solutions is impossible at the large Taylor numbers dealt with in this paper.

The finite-amplitude instability for weakly nonlinear convection has not been observed in our numerical analysis. It is, however, a common phenomenon in a system constrained externally by rotation that the bifurcation exhibits subcritical behaviour. Such subcritical instabilities were found in a rotating plane layer (Veronis 1965) and in a rotating magnetohydrodynamic system (Soward 1974). In order to have a subcritical bifurcation, nonlinear effects are usually able to provide a mean to offset the externally imposed constraint and to effectively relax parts of the constraint. Although the finite-amplitude effects for $Pr \leqslant 1$ are dramatically strong in terms of the amplitude of the generated mean flow, the nearly z-independent structure minimizes the controlling constraint imposed by rotation. A supercritical bifurcation with this type of nonlinear solution is therefore not surprising. It is important to note that strong zonal flows are suppressed in Soward's model (1977) by the Ekman suction, which is absent in our model with stress-free boundaries. This may explain why the finite-amplitude instability, suggested by Soward (1977), has not been found in our analysis. For large Prandtl numbers, nonlinear interactions between different components of the velocity are too weak to produce any substantial effects which may relax the constraint of rotation.

6. Concluding remarks

A prominent feature of convection emerging from our results, in contrast with previous analysis, is the strong dependence of both small- and finite-amplitude convection on the size of the Prandtl number of a fluid. It is the combined influences of the Coriolis forces, the spherical boundary curvature and the effects of the Prandtl number that play a crucial role in determining the properties of convection in rotating spherical fluid systems. The most important finding of this paper is the novel relationship between the spiralling columnar instability and large-amplitude zonal flows. Explanations are proposed to account for a dominantly axisymmetric zonal flow in rapidly rotating spherical fluid systems which choose small-scale non-axisymmetric motions at the onset of convection.

Our numerical analysis leads to a somewhat more complicated picture for the analytic approach to the linear problem owing to the fact that the form of linear solutions depends critically on the Prandtl number. The previous asymptotic linear theories are considerably simplified by the assumption of the domination of $\partial/\partial\phi$. This assumption appears most seriously violated for the fluids with moderately small Prandtl numbers. It is suggested that the important mathematical advantage associated with a shorter azimuthal scale cannot be taken for the general problem. On the other hand, the structure of linear convection can be resolved if $\partial/\partial s$ is retained in the analysis.

It has been a challenge to geophysical fluid dynamicists to find an interpretation of observed features such as the dominantly axisymmetric equatorial zonal jets exhibited by the atmospheres of giant planets in terms of basic fluid dynamical process. The central theoretical effort in most of the earlier studies of nonlinear convection in rotating spherical bodies was in connection with the generation of mean zonal flows. Lack of precise information about the interior properties makes it very difficult to integrate the hydrodynamic equations numerically to simulate realistic flows, even on the largest computers available. For this reason, our efforts have centred on simplified models which we believe contain the essential physics while being tractable numerically by following the sequence of bifurcation. Our preliminary findings should be regarded as important for the heuristic character of rotating convection in spherical systems, not for its application to the detailed explanation of specific phenomena. Since the fluid of many systems like Jupiter is eventually characterized by lower Prandtl numbers, the finding of the relationship between the spiralling columnar mode and the equatorial zonal jets will certainly lead to a better understanding of the hydrodynamic processes taking place. It cannot be claimed at the present stage that the spiralling columnar convection is the mechanism which produces the equatorial zonal flows observed in the major planets. However, the combined effects of strong Coriolis forces, spherical boundary geometry and lower Prandtl numbers, as described in this paper, undoubtedly play an important part in the hydrodynamic processes which produce the zonal jets.

A great deal can be learnt through studying the instability properties of the nonlinear solutions at larger Rayleigh numbers where the fast equatorial zonal flow is likely to be saturated by a mechanism in the form of hydrodynamic instabilities. But the instability properties and higher bifurcations of the nonlinear solutions associated with the spiralling columnar convection can only be studied at relatively small Taylor numbers.

I would like to thank the Leverhulme Trust for a Research Fellowship. I would also like to express my gratitude to Professor F. H. Busse and especially Professor A. M. Soward for useful discussions. I wish to take this opportunity to thank Professor P. H. Roberts for many helpful discussions about the subject when I was at UCLA.

REFERENCES

BUSSE, F. H. 1970*a* Thermal instabilities in rapidly rotating systems. *J. Fluid Mech.* **44**, 441–460.

BUSSE, F. H. 1970*b* Differential rotation in stellar convection zones. *Astrophys. J.* **159**, 620–639.

BUSSE, F. H. 1976 A simple model of convection in Jovian atmosphere. *Icarus* **20**, 255–260.

BUSSE, F. H. 1983 A model of mean flows in the major planets. *Geophys. Astrophys. Fluid Dyn.* **23**, 152–174.

BUSSE, F. H. & CUONG, P. G. 1979 Convection in rapidly rotating spherical fluid shells. *Geophys. Astrophys. Fluid Dyn.* **8**, 17–41.

CARRINGAN, C. R. & BUSSE, F. H. 1983 An experimental and theoretical investigation of the onset of convection in rotating spherical shells. *J. Fluid Mech.* **126**, 287–305.

CHAMBERLAIN, J. A. & CARRIGAN, C. R. 1986 An experimental investigation of convection in a rotating sphere subject to time varying thermal boundary conditions. *Geophys. Astrophys. Fluid Dyn.* **41**, 17–41.

CHANDRASEKHAR, S. 1961 *Hydrodynamic and Hydromagnetic Stability*. Oxford: Clarendon Press.

FEARN, D. R. 1979*a* Thermally driven hydrodynamic convection in a rapidly rotating sphere. *Proc. R. Soc. Lond.* A **369**, 227–242.

FEARN, D. R. 1979*b* Thermal and magnetic instabilities in a rapidly rotating sphere. *Geophys. Astrophys. Fluid Dyn.* **14**, 103–126.

FEARN, D. R., ROBERTS, P. H. & SOWARD, A. M. 1988 Convection, stability and the dynamo. In *Energy, Stability and Convection* (ed. B. Straughan & P. Galdi), pp. 60–324. Longman.

GILMAN, P. A. 1977 Nonlinear dynamics of Boussinesq convection in a deep rotating spherical shell. I. *Geophys. Astrophys. Fluid Dyn.* **8**, 93–135.

GLATZMAIER, G. A. 1983 Numerical simulations of stellar convective dynamos. I. The model and method. *J. Comp. Phys.* **55**, 461–484.

HART, J. E., GLATZMAIER, G. A. & TOOMRE, J. 1986 Space-laboratory and numerical simulations of thermal convection in a rotating hemispherical shell with radial gravity. *J. Fluid Mech.* **173**, 519–544.

INGERSOLL, A. P., BEEBE, R. F., COLLINS, S. A., HUNT, G. E., MITCHELL, J. L., MULLER, J. P., SMITH, B. A. & TERRILE, R. J. 1981 Zonal velocity and texture in the Jovian atmosphere inferred from Voyager images. *Nature* **280**, 773–775.

MOFFATT, H. K. 1978 *Magnetic Field Generation in Electrically Conducting Fluids.* Cambridge University Press.

ROBERTS, P. H. 1965 On the thermal instability of a highly rotating fluid sphere. *Astrophys. J.* **141**, 240–250.

ROBERTS, P. H. 1968 On the thermal instability of a self-gravitating fluid sphere containing heat sources. *Phil. Trans. R. Soc. Lond.* A**263**, 93–117.

SOWARD, A. M. 1974 A convection-driven dynamo. I. Weak field case. *Phil. Trans. R. Soc. Lond.* A**272**, 431–462.

SOWARD, A. M. 1977 On the finite amplitude thermal instability of a rapidly rotating fluid sphere. *Geophys. Astrophys. Fluid Dyn.* **9**, 19–74.

VERONIS, G. 1966 Motions at subcritical values of the Rayleigh number in a rotating fluid. *J. Fluid Mech.* **24**, 545–554.

ZHANG, K. & BUSSE, F. 1987 On the onset of convection in rotating spherical shells. *Geophys. Astrophys. Fluid Dyn.* **39**, 119–147.

ZHANG, K. & BUSSE, F. 1989 Convection driven magnetohydrodynamic dynamos in rotating spherical shells. *Geophys. Astrophys. Fluid Dyn.* **49**, 97–116.